Supplementary Information (SI) for Inorganic Chemistry Frontiers.

Supporting Information for

In-situ Electrodeposition of Pt into a Trimetallic MOFs Composite Electrode and Its Application in Water Splitting

Tianpeng Liu[a], Xin Wang[a], Jie Li[a], Mengyun Hu[a], Jun Yu[a], Shudi Yu[a], Zhengying Wu[b]*, Yukou Du[a]*

[a] *College of Chemistry, Chemical Engineering and Materials Science, Soochow University, Industrial Park, Renai Road, Suzhou 215123, P.R. China*

[b] *Jiangsu Key Laboratory for Environment Functional Materials, School of Materials Science and Engineering, Suzhou University of Science and Technology, Suzhou 215009, China*

E-mail: duyk@suda.edu.cn (Y. Du), zywu@mail.usts.edu.cn (Z. Wu).

Entry	Title	Page No.
Experimental	Synthesis of trimetallic composite electrodes.	3
	Synthesis of FeNiCoPt/NF composite electrode.	3
	Materials and chemicals	4
	Physical Characterizations	4
	Electrochemical measurements	4
Fig. S1	Elemental composition analysis of FeNiCo/NF and FeNiCoPt	**6**
Fig. S2	XRD pattern of trimetallic MOF (FeNiCo, FeNiZn) and Fe-MIL100.	**6**
Fig. S3	High-resolution XPS spectra of FeNiCo/NF: (a) survey scan, (b) Fe 2p, (c) Ni 2p and (d) Co 2p.	**7**
Fig. S4	CV curves for the non-Faraday interval: (a) FeNiCo/NF, (b) FeNiZn/NF, (c) FeNiCoPt/NF, (d) RuO_2, and (e) C_{dl} values of electrode materials.	**7**
Table. S1	Charge-transfer resistors of composite electrodes in OER and HER.	**8**
Fig. S5	CV curves for the non-Faraday interval: (a) FeNiCo/NF, (b) FeNiZn/NF, (c) FeNiCoPt/NF, (d) Pt/C. (e) C_{dl} values of each electrode materials.	**8**
Fig. S6	Changes in the D-band center of FeNiCoPt/NF before and after testing.	**8**
Fig. S7	Comparison of overall water splitting performance (j=100 mA cm^{-2}).	**9**
Table. S2	Working voltage of the two-electrode system driving OWS at 100 mA cm-2	**9**
References		**10**

Experimental

Synthesis of trimetallic composite electrodes.

The synthesis of the trimetallic composite electrode material was adapted from prior research. The procedure commenced with the meticulous cleaning of commercial nickel foam (NF) to eliminate surface organic contaminants and oxides. The cleaning protocol involved soaking the trimmed NF (1cm × 1 cm) in acetone, subjecting it to 15 minutes of ultrasonic agitation, and subsequently rinsing it with ethanol and deionized water to purge residual organics and acetone. Subsequently, NF was immersed in 3 mol/L HCl solution and sonicated for 15 min before being rinsed again with ethanol and deionized water to remove the oxide and HCl solution from the surface. Finally, the cleaned NF was placed under an infrared lamp to dry for use.

A solvothermal synthesis approach was employed for FeNiCo composite electrode growth: 0.162 mmol $Fe(NO_3)_3·9H_2O$ (65.6 mg), 0.324 mmol $Ni(NO_3)_2·6H_2O$ (94.5 mg), and 0.162 mmol $Co(NO_3)_2·6H_2O$ (47.3 mg) were dissolved in 8 mL anhydrous *N,N*-dimethylformamide (DMF) under 30 min ultrasonication and labeled as solution A. In addition, 1, 3, 5-trimesic acid (H_3BTC,102.5 mg, 0.487 mmol) powder was dissolved in 8 mL DMF, sonicated for 30 min at room temperature and labeled as solution B. The above solution A was mixed with solution B and sonicated for 30 min at room temperature, then the mixed solution was transferred to a Teflon autoclave and reacted at 170 ◦C for 24 h. After cooling at room temperature, the products were removed, purified by washing with ethanol and water respectively, centrifuged three times, and finally dried at 60 ◦C labeled FeNiCo/NF. The FeNiZn/NF composite electrode was prepared in a similar way to FeNiCo/NF, and only $Co(NO_3)_2·6H_2O$ in the reactant was replaced by $Zn(NO_3)_2·6H_2O$.

Synthesis of FeNiCoPt/NF composite electrode.

FeNiCoPt/NF electrode was prepared by electrochemical deposition as follows: Potassium chloroplatinate (K_2PtCl_6) crystal was dissolved in deionized water to prepare an orange K_2PtCl_6 solution with a concentration of 3.86 mmol/L. Subsequently, the newly prepared FeNiCo/NF was fixed with a platinum sheet electrode clamp and immersed in the H_2PtCl_6 solution described above. Electrodeposition was performed by cyclic voltammetry with a scan range of -0.25 to

0.80 V (vs. Ag/AgCl), 20 scan segments, and a scan rate of 50 mV/s. After electrodeposition, rinse with deionized water and dry at 60 ◦C before use[1].

Materials and chemicals

Cobalt (II) nitrate hexahydrate ($Co(NO_3)_2 6H_2O$, A.R.), Iron (III) nitrate hexahydrate ($Fe(NO_3)_3$ $9H_2O$, A.R.), Nickel (II) nitrate hexahydrate ($Ni(NO_3)_2$ $6H_2O$, A.R.) and Potassium chloroplatinate (K_2PtCl_6, A.R.) were obtained from Sinopharm Chemicals Reagent Co., Ltd, China. Nafion (5% wt), 1, 3, 5-trimesic acid (H_3BTC, 99%), *N, N*-Dimethylformamide (DMF, 99.5%), and Potassium hydroxide (KOH, G.R.) were purchased from Sigma−Aldrich., ethanol (A.R.) was purchased from Alfa Aesar.

Physical Characterizations

The surface elemental valence states of the samples were determined by X-ray photoelectron spectroscopy (XPS, EXCALAB 250 XI). The elemental composition and phases of the electrocatalysts were obtained by scanning electron microscope (SEM, EVO18) and X-ray diffraction (XRD, X Pert-Pro MPD). The microscopic morphology of the samples was obtained by Transmission electron microscope (TEM, HT-7700) and High-resolution Transmission electron microscope (HRTEM, Talos F200X G2).

Electrochemical measurements

All electrochemical experiments were collected by the electrochemical workstation (CHI 760E Chenhua, Shanghai) in 1 mol/L KOH alkaline solution at room temperature. The electrodes in the electrochemical tests are working electrode (nickel foam electrode, area 1×1 cm), counter electrode (carbon rod), and reference electrode (Ag/AgCl), respectively.

All potentials were converted to reversible hydrogen potentials using the following formula (RHE): E (RHE) = E (Ag/AgCl) + 0.197 + 0.059 × pH. The test parameters of LSV were as follows: initial potential 0 V, termination potential 0.7 V, sweep speed 5 mV s^{-1}. In addition, 95% iR compensation was used to correct the electrochemical tests to eliminate the interference of solution internal resistance to the experiment.

The capacitance of the electric double layer of the electrode material was first calculated by CV curve at different sweep speeds, and then ECSA was calculated by combining the capacitance per unit area of the material. The details are as follows:

ECSA=C_{dl}/C_s Where C_{dl} represents the capacitance of the electrical double layer, and C_s represents the specific capacitance of the sample or the capacitance of the smooth plane of the material per unit area under the same electrolyte conditions. Based on previous reports, we used C_s = 0.035 mF cm^{-2} (1 mol/L H_2SO_4) and Cs = 0.040 mF cm^{-2} (1 mol/L NaOH) as specific charges for evaluating the catalytic material ECSA Capacity. The ECSA-normalized LSV curve is calculated by the following formula: j_{ECSA} = j/ECSA Where j_{ECSA} represents the normalized current density, j represents the actual tested current density, and ECSA represents the electrochemical active area.

Supporting Figure and Tables

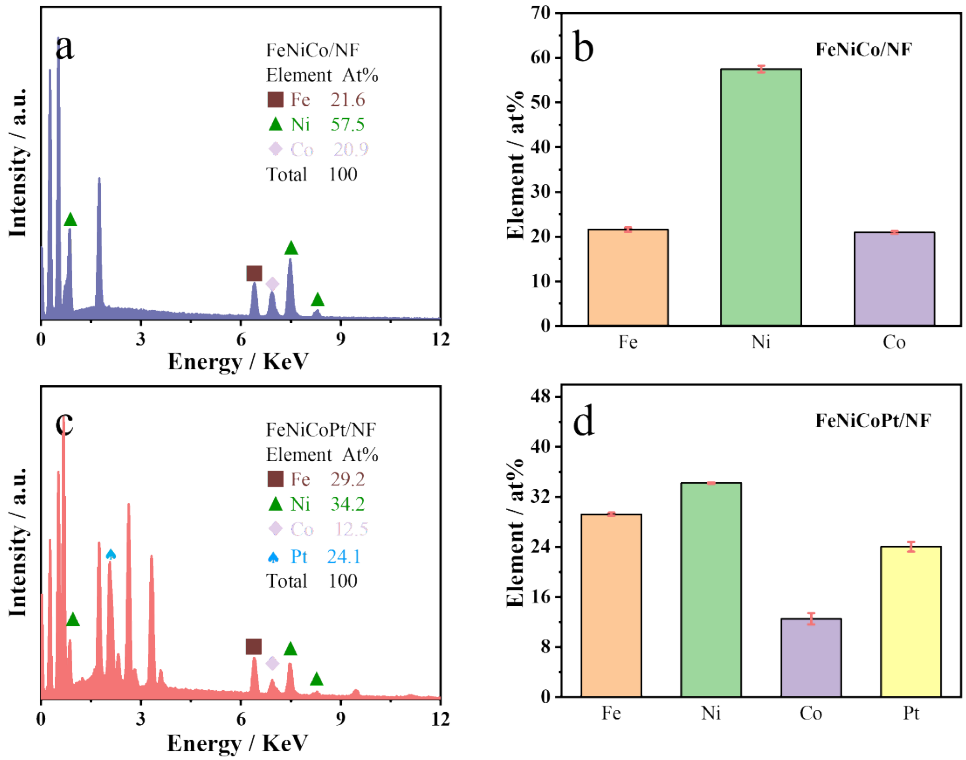

Figure. S1 Elemental composition analysis of FeNiCo/NF: (a) EDS and (b) error analysis. Elemental composition analysis of FeNiCoPt/NF: (c) EDS and (d) error analysis.

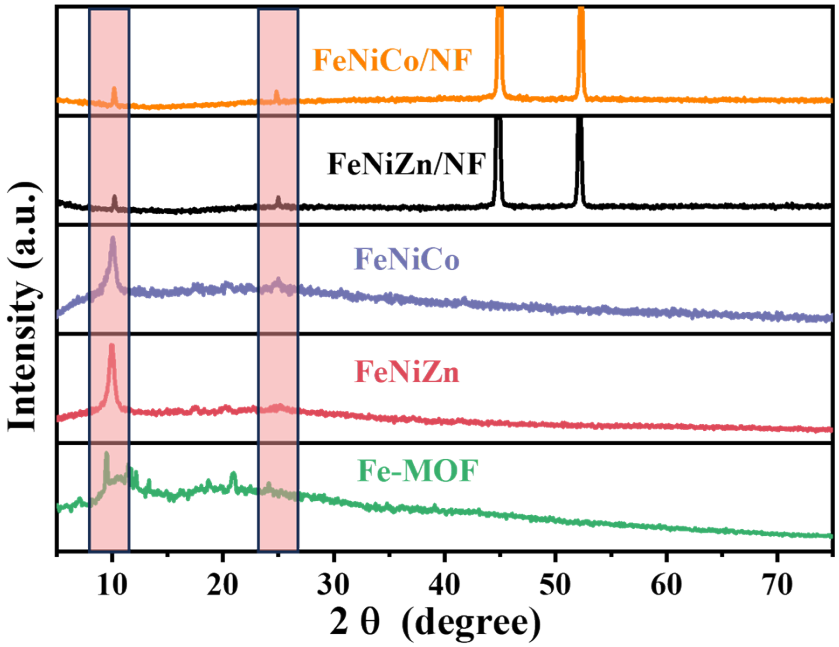

Figure. S2 XRD pattern of trimetallic MOF (FeNiCo, FeNiZn, FeNiCo/NF and FeNiZn/NF) and Fe-MOF.

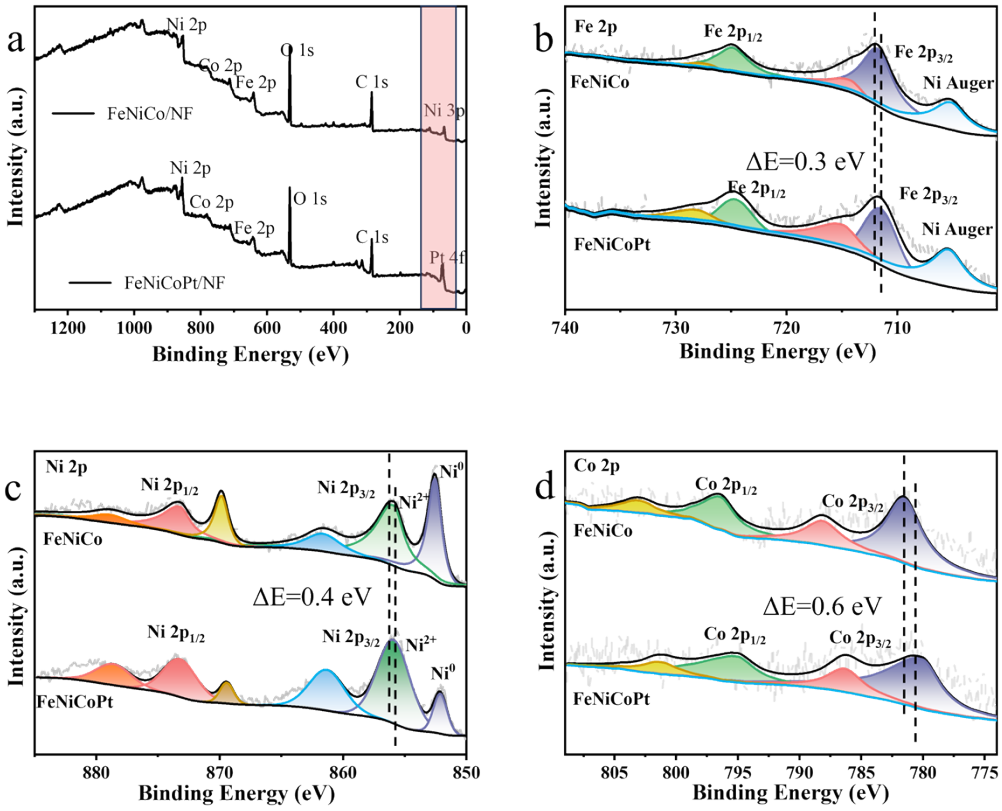

Figure. S3 High-resolution XPS spectra of FeNiCo/NF: (a) survey scan, (b) Fe 2p, (c) Ni 2p and (d) Co 2p.

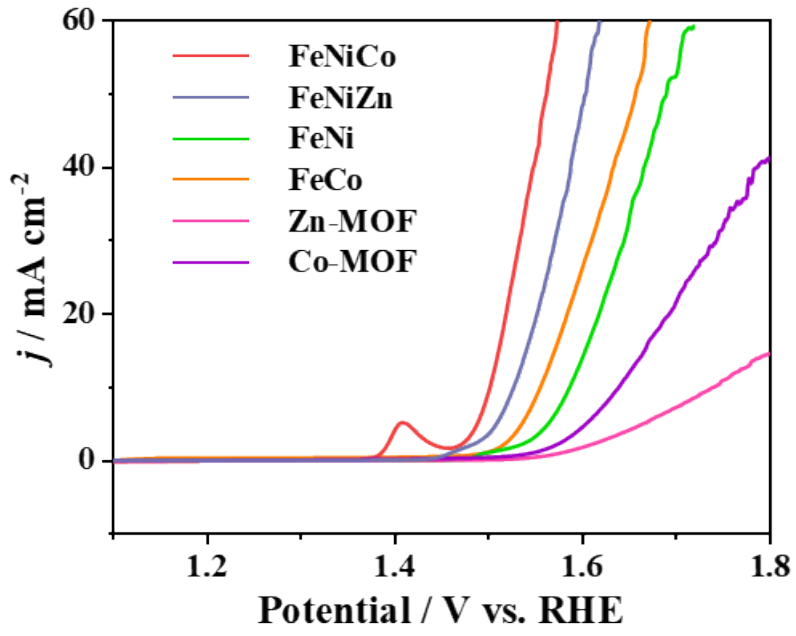

Figure. S4. LSV curves of monometallic MOFs, bimetallic MOFs and trimetallic MOFs.

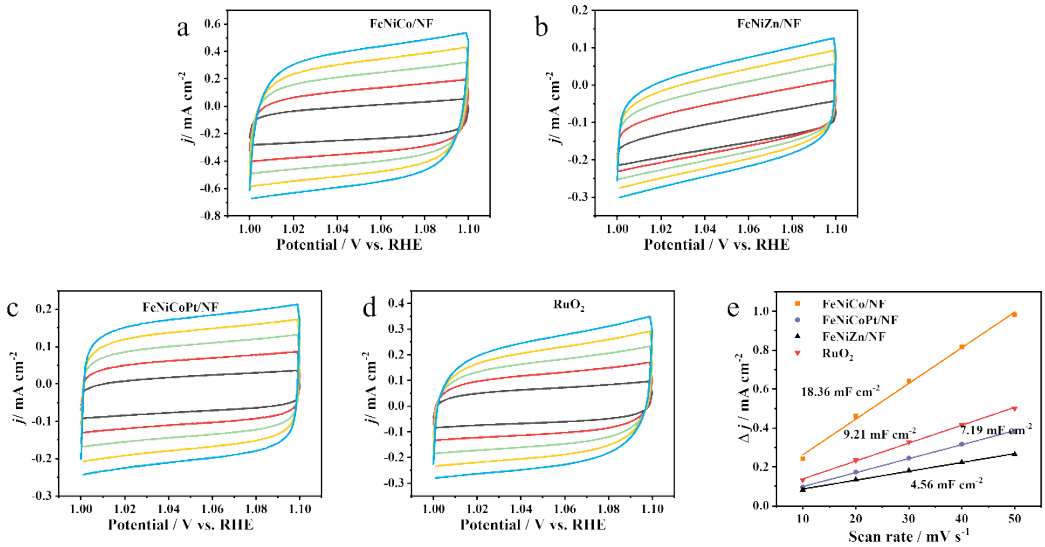

Figure. S5. CV curves for the non-Faraday interval: (a) FeNiCo/NF, (b) FeNiZn/NF, (c) FeNiCoPt/NF, (d) RuO_2, and (e) C_{dl} values of electrode materials.

Table. S1 Charge-transfer resistors of composite electrodes in OER and HER.

Catalysts	R_{ct} / Ω（OER）	R_{ct} / Ω（HER）
FeNiCo/NF	2.26	9.79
FeNiZn/NF	4.89	15.4
FeNiCoPt/NF	6.24	7.62
RuO_2	67.83	-----
Pt/C	-----	12.47

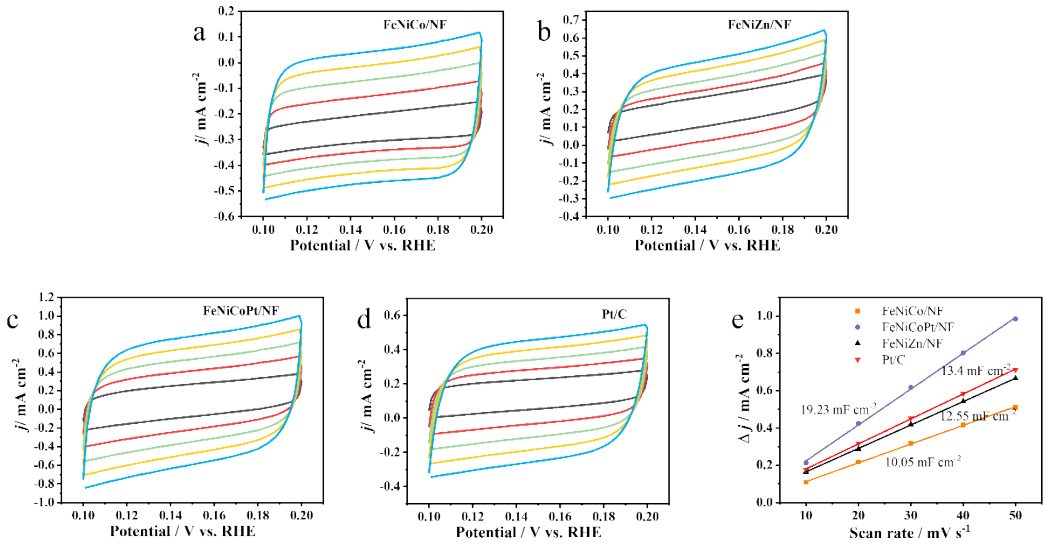

Figure. S6 CV curves for the non-Faraday interval: (a) FeNiCo/NF, (b) FeNiZn/NF, (c) FeNiCoPt/NF, (d) Pt/C. (e) C_{dl} values of each electrode materials.

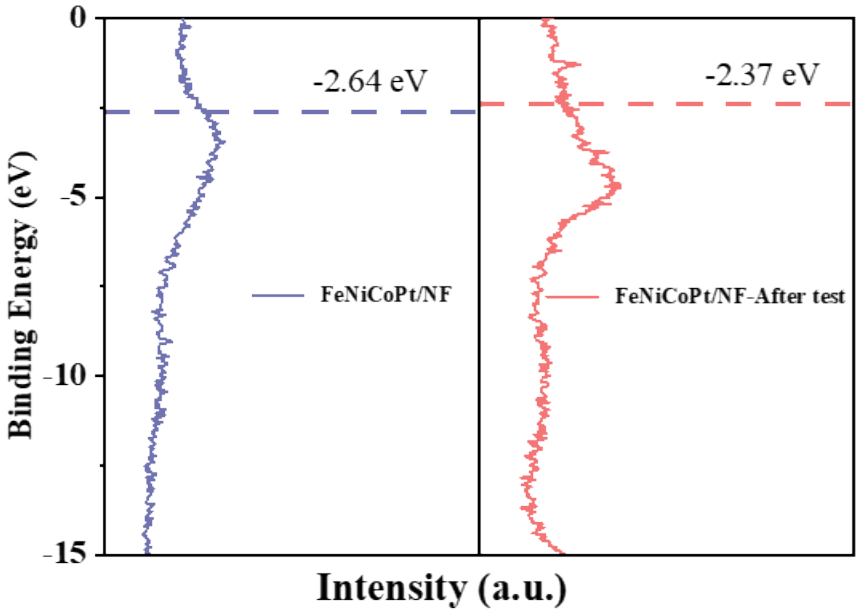

Figure. S7 Changes in the D-band center of FeNiCoPt/NF before and after testing.

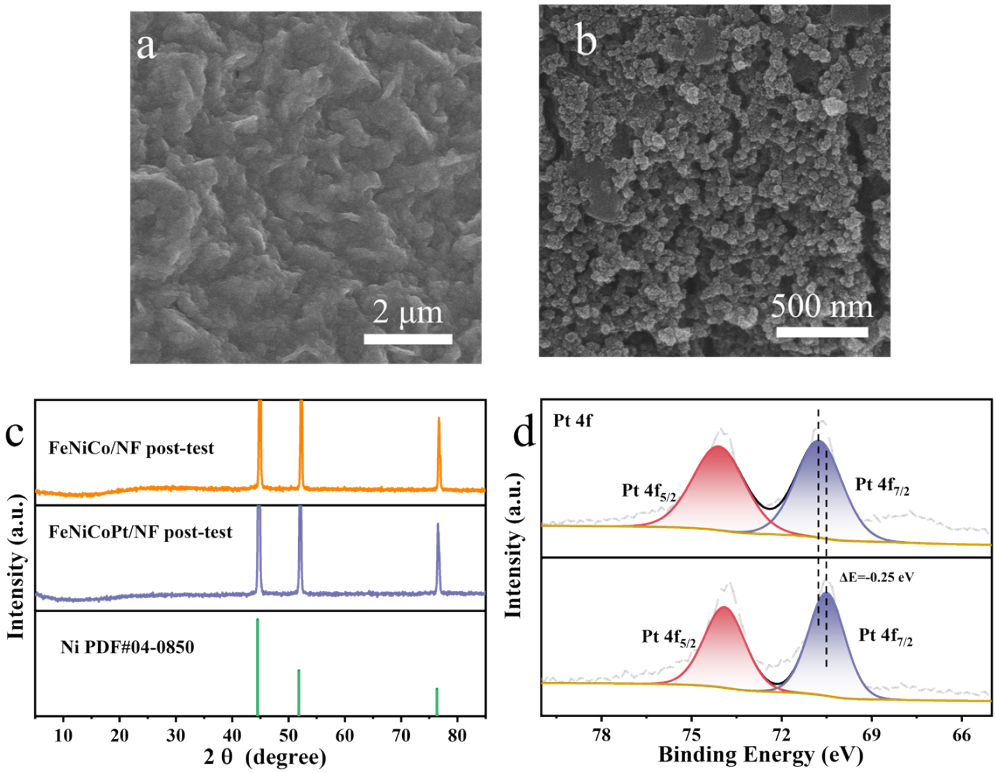

Figure. S8 Comparison of overall water splitting performance (j=100 mA cm^{-2}).

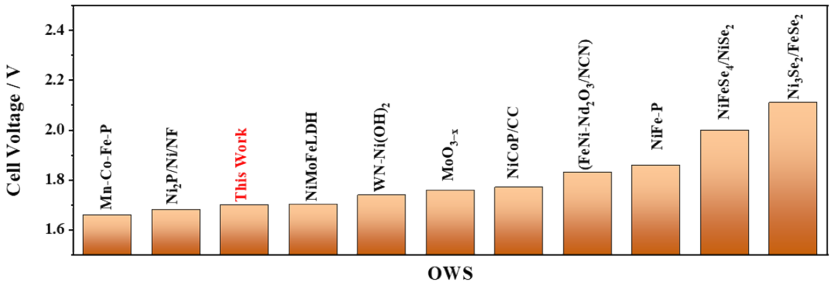

Figure. S9 Comparison of overall water splitting performance (j=100 mA cm^{-2}).

Table S2 Working voltage of the two-electrode system driving OWS at 100 mA cm^{-2}

Catalysts	voltage / V	References
Mn-Co-Fe-P	1.66	2
Ni_2P/Ni/NF	1.68	3
NiMoFeLDH	1.702	4
WN-$Ni(OH)_2$	1.74	5
MoO_{3-x}	1.76	6
NiCoP/CC	1.77	7
FeNi-Nd_2O_3/NCN	1.83	8
NiFe-P	1.86	9
$NiFeSe_4/NiSe_2$	2.0	10
$Ni_3Se_2/FeSe_2$	2.11	11

References

1. J. Yin; C. Wang; J. Li; S. Yu; Z. Wu; Y. Zhang; Y. Du. In situ electrodeposition of ultralow Pt into NiFe-Metal-Organic Framework/nickel foam nanosheet arrays as a bifunctional catalyst for overall water splitting. *Inorg. Chem.* **2024**, 63 (11), 5167-5174. DOI: 10.1021/acs.inorgchem.4c00124.
2. F. Wang; Z. Pei; Z. Xu; T. Qin; X. Ouyang; D. Li; Y. Hou; X. Guo. Constructing Mn-Co-Fe ternary metal phosphides nanosheet arrays as bifunctional electrocatalysts for overall water splitting. *Adv. Sci.* **2025**. DOI: 10.1002/advs.202417521.
3. B. You; N. Jiang; M. Sheng; M. W. Bhushan; Y. Sun. Hierarchically porous urchin-like Ni2p superstructures supported on nickel foam as efficient bifunctional electrocatalysts for overall water splitting. *ACS Catal.* **2016**, 6 (2), 714-721. DOI: 10.1021/acscatal.5b02193.
4. Q. Zhang; W. Xiao; J. X. Shi; J. L. Lei; Q. Xiao; H. Q. Luo; N. B. Li. Dynamic molybdate oxyanion boosts self-optimization and self-healing on the NiMoFe heterostructure for water splitting in alkaline media. *ACS Catal.* **2024**, 14 (23), 18003-18017. DOI: 10.1021/acscatal.4c05108.
5. C. Lv; X. Wang; L. Gao; A. Wang; S. Wang; R. Wang; X. Ning; Y. Li; D. W. Boukhvalov; Z. Huang; C. Zhang. Triple functions of $Ni(OH)_2$ on the surface of Wn nanowires remarkably promoting electrocatalytic activity in full water splitting. *ACS Catal.* **2020**, 10 (22), 13323-13333. DOI: 10.1021/acscatal.0c02891.
6. D. Feng; P. Wang; R. Qin; W. Shi; L. Gong; J. Zhu; Q. Ma; L. Chen; J. Yu; S. Liu; S. Mu. Flower-like amorphous MoO_{3-x} stabilized ru single atoms for efficient overall water/seawater splitting. *Adv. Sci.* **2023**, 10 (18). DOI: 10.1002/advs.202300342.
7. C. Du; L. Yang; F. Yang; G. Cheng; W. Luo. Nest-like NiCoP for highly efficient overall water splitting. *ACS Catal.* **2017**, 7 (6), 4131-4137. DOI: 10.1021/acscatal.7b00662.
8. J. Li; Y. Qin; T. Tan; Q. Zhu; B. Ouyang; E. Kan; W. Zhang. Enhancing the activity of FeNi bimetallic electrocatalysts on overall water splitting by Nd_2O_3-induced FeNi lattice contraction. *J. Energy Chem.* **2023**, 87, 42-50. DOI: https://doi.org/10.1016/j.jechem.2023.08.021.
9. J. Wang; L. Ji; S. Zuo; Z. Chen. Hierarchically structured 3d integrated electrodes by galvanic replacement reaction for highly efficient water splitting. *Adv. Energy Mater.* **2017**, 7 (14), 1700107. DOI: 10.1002/aenm.201700107.
10. L. Mu; S. Qiu; G. Zhao; B. Zhang; W. Liao; N. Zhao; X. Xu. A high-efficiency $NiFeSe_4/NiSe_2$ bifunctional electrocatalyst with outstanding oxygen evolution reaction and overall water splitting performance. *J. Mater. Chem. A* **2024**, 12 (3), 1714-1724. DOI: 10.1039/d3ta06701g.
11. L. Guo; T. Liu; L. Zhang; M. Ma; P. Gao; D. Cao; D. Cheng. Novel $Ru\text{-}O_3Se_4$ single atoms regulate the charge redistribution at $Ni_3Se_2/FeSe_2$ interface for improved overall water splitting in alkaline media. *Adv. Energy Mater.* **2025**, 15 (1). DOI: 10.1002/aenm.202402558.